

Pure-quartic soliton molecules in normal fourth-order dispersion regimes based on spectral filtering effect

Han-Yang Shen(申翰阳), Rui-Bo Lan(蓝睿博), Hong-Bin Hu(胡洪彬), Yang Li(李阳), Rui Zhou(周瑞), and Zu-Xing Zhang(张祖兴)†

Citation: Chin. Phys. B, 2025, 34 (**3**): 034203. DOI: 10.1088/1674-1056/ada43c
Journal homepage: http://cpb.iphy.ac.cn; http://iopscience.iop.org/cpb

What follows is a list of articles you may be interested in

Femtosecond mode-locking and soliton molecule generation based on a GaAs saturable absorber

Chen-Yan Zhang(张辰妍), Xin-He Dou(窦鑫河), Zhen Chen(陈震), Jing-Han Zhao(赵靖涵), Wei Sun(孙薇), Ze-Yu Fan(樊泽宇), Tao Zhang(张涛), Hao Teng(滕浩), and Zhi-Guo Lv(吕志国)

Chin. Phys. B, 2025, 34 (**1**): 014205. DOI: 10.1088/1674-1056/ad8db3

Dissipative soliton resonance within different dispersion regimes in a single mode-locked laser

Zhetao Zhao(赵哲韬), Qinke Shu(舒沁珂), Ziyi Xie(解梓怡), Yuxuan Ren(任俞宣), Ying Zhang(张颖), Bo Yuan(袁博), Chunbo Zhao(赵春勃), Junsong Peng(彭俊松), and Heping Zeng(曾和平)

Chin. Phys. B, 2024, 33 (**7**): 074208. DOI: 10.1088/1674-1056/ad47b1

Comprehensive analysis of pure-quartic soliton dynamics in a passively mode-locked fiber laser

Lie Liu(刘列), Ying Han(韩颖), Jiayu Huo(霍佳雨), Honglin Wen(文红琳), Ge Wu(吴戈), and Bo Gao(高博)

Chin. Phys. B, 2023, 32 (**11**): 114209. DOI: 10.1088/1674-1056/acc451

Real-time observation of soliton pulsation in net normal-dispersion dissipative soliton fiber laser

Xu-De Wang(汪徐德), Xu Geng(耿旭), Jie-Yu Pan(潘婕妤), Meng-Qiu Sun(孙梦秋), Meng-Xiang Lu(陆梦想), Kai-Xin Li(李凯芯), and Su-Wen Li(李素文)

Chin. Phys. B, 2023, 32 (**2**): 024210. DOI: 10.1088/1674-1056/ac76b0

Generation of high-energy dual-wavelength domain wall pulse with low repetition rate in an HNLF-based fiber ring laser

Luo Zhi-Chao (罗智超), Lin Zhen-Bin (林振彬), Li Jin-Yu (李金玉), Zhu Peng-Fei (朱鹏飞), Ning Qiu-Yi (宁秋奕), Xing Xiao-Bo (邢晓波), Luo Ai-Ping (罗爱平), Xu Wen-Cheng (徐文成)

Chin. Phys. B, 2014, 23 (**6**): 064203. DOI: 10.1088/1674-1056/23/6/064203

Pure-quartic soliton molecules in normal fourth-order dispersion regimes based on spectral filtering effect

Han-Yang Shen(申翰阳), Rui-Bo Lan(蓝睿博), Hong-Bin Hu(胡洪彬), Yang Li(李阳), Rui Zhou(周瑞), and Zu-Xing Zhang(张祖兴)†

Advanced Photonic Technology Laboratory, College of Electronic and Optical Engineering & College of Flexible Electronics (Future Technology), Nanjing University of Posts and Telecommunications, Nanjing 210023, *China*

(Received 14 November 2024; revised manuscript received 27 December 2024; accepted manuscript online 31 December 2024)

Recent theoretical verification of self-similar and dissipative pure-quartic solitons (PQSs) emphasized the similarity between PQS lasers and conventional fiber lasers, but the unique equilibrium mechanism hinders the formation of PQS molecules in normal fourth-order dispersion (FOD) regimes. In this paper, we investigated the effect of filters on shaping PQSs in normal FOD based on a passively mode-locked fiber laser model. A bandpass filter eliminates the time pedestal of dissipative PQSs, thus realizing a multi-pulsing state. When the filter bandwidth is appropriate, the effective spectral filtering effect can lower the pulse splitting threshold and enable the coherent restoration from chaotic PQSs to PQS molecules. Additionally, changing the central wavelength of the filter can generate PQSs and PQS molecules with asymmetric intensity distributions. These results are important guides for the manipulation of PQSs and the construction of high repetition-frequency fiber lasers.

Keywords: pure-quartic soliton, soliton molecule, spectral filtering effect, mode-locked fiber laser

PACS: 42.65.Sf, 42.65.Tg, 42.55.Wd, 42.60.Fc

DOI: 10.1088/1674-1056/ada43c **CSTR:** 32038.14.CPB.ada43c

1. Introduction

Optical solitons in passively mode-locked fiber lasers (PMFLs) are self-localized wave packets, whose discovery has been applied to many novel optical applications, including ultrafast laser technology,[1–3] optical frequency combs,[4–6] and telecommunications and signal processing.[7–9] Initially, the formation of solitons was thought to be balanced between anomalous dispersion and nonlinear effects. However, limited by the soliton area theorem, the energy of conventional solitons is only on the order of pico-Joules. The dispersion management method of arranging the fibers with positive and negative dispersion alternately can be used to obtain soliton outputs with different energies at different locations in the cavity, i.e., dispersion-managed solitons.[10] Inspired by dispersion management, self-similar and dissipative solitons in the positive dispersion region have been successfully realized, which breaks through the energy limitations by balancing the dispersion, nonlinearity, gain, loss, spectral filtering, and other effects, thus increasing the soliton energy by several orders of magnitude. Traditionally, dispersion engineering regulates second-order dispersion (SOD) in the cavity. Due to the development of fiber optics and spatial dispersion engineering, this concept has been extended to fourth-order dispersion (FOD) or higher even-order dispersion.[11] After the first discovery of pure-quartic solitons (PQSs) in photonic crystal waveguides in 2016,[12] they have been widely investigated because of the significant enhancement of energy for ultrashort pulses and the unique equilibrium mechanism. Then, not only were conventional PQSs realized in PMFLs,[13] but also self-similar and dissipative PQSs were obtained at normal FOD regimes,[14–16] which exhibited similar output patterns to conventional PMFLs.

The formation of multiple pulses is a well-known phenomenon in PMFLs. Affected by the peak clamping effect, the unstable modulation of the noise seed at high pump power causes soliton splitting.[17] When the splitting solitons are tightly bound through interactions, they form bound-state soliton molecules or even molecular complexes, exhibiting properties similar to those of matter molecules.[18] If the soliton separation is appropriate, harmonic mode-locking may occur, which greatly increases the repetition frequency of the PMFL. Therefore, soliton splitting is desired for studying soliton interactions and constructing high repetition frequency PMFLs. Compared to conventional solitons, although the PQS has a higher splitting threshold because the pulse tails can create potential barriers to provide strong repulsive force,[19] it can still split to form PQS molecules under the overdriven nonlinear effect. The additional interactions of the pulse tails render the evolution of PQS molecules both intriguing and compelling, thus triggering related studies about pulsating PQS molecules,[20] vector PQS molecules,[21] and PQS molecular interactions.[22] However, the above studies of PQS molecules were carried out at net anomalous FOD. The multiple soliton states at normal FOD have not yet been obtained, since self-

†Corresponding author. E-mail: zxzhang@njupt.edu.cn

© 2025 Chinese Physical Society and IOP Publishing Ltd. All rights, including for text and data mining, AI training, and similar technologies, are reserved.

similar and dissipative PQS exhibit resonance or asymmetric features rather than splitting at high energies.[15,23]

In the present work, we realized PQS molecules in normal FOD regimes based on a PMFL model. The PMFL outputs dissipative PQSs without the filter. When adding a bandpass filter to impose effective spectral filtering, the PMFL can generate PQS molecules consisting of one to five PQSs. Further optimization of the filter bandwidth allows the PMFL to recover from chaotic PQSs to coherent multi-pulsing states. Moreover, adjusting the central wavelength of the filter enables PMFL to output PQSs that exhibit asymmetric shapes in temporal and spectral domains. These outcomes highlight the critical role of the spectral filtering effect in generating PQS molecules in normal FOD regimes and provide new insights for the dynamic control of multi-soliton states and the construction of high repetition frequency PQS lasers.

2. Numerical method

Our results are based on a typical PMFL model, with Fig. 1 illustrating its fundamental structure. The cavity consists of Er-doped fibers (EDFs), a saturable absorber (SA), a spectral filter, an output coupler (OC), and a spectral pulse shaper (SPS). These elements are connected using single-mode fibers (SMFs). The propagation dynamics of solitons are described by the nonlinear Schrödinger equation (NLSE), which is typically of the form[24]

$$\frac{\partial A}{\partial z} = -\frac{\mathrm{i}\beta_2}{2}\frac{\partial^2 A}{\partial t^2} + \frac{\beta_3}{6}\frac{\partial^3 A}{\partial t^3} + \frac{\mathrm{i}\beta_4}{24}\frac{\partial^4 A}{\partial t^4} + \mathrm{i}\gamma|A|^2 A + \frac{g-\alpha}{2}A, \tag{1}$$

where A represents the slowly varying amplitude of the pulse envelope, z is the propagation distance. β_2, β_3, and β_4 symbolize SOD, third-order dispersion (TOD), and FOD of the fiber, respectively, t is the time coordinate. γ is the nonlinear coefficient. g and α are the gain and loss coefficients of the fiber, respectively, where g is related to the pulse energy and can be expressed as[25]

$$g = \frac{g_0}{1 + \int |A(z,t)|^2 \,\mathrm{d}t / E_{\mathrm{sat}} + \left(\omega/\Omega_{\mathrm{g}}\right)^2}, \tag{2}$$

where g is the small-signal gain coefficient and E_{sat} is the saturation energy of EDFs. ω is the angular frequency. Ω_{g} is the gain bandwidth of the EDFs.

The transmittance equation of the SA is related to the pulse intensity, which can be written as

$$T = 1 - \frac{q_0}{1 + |A(z,t)|^2 / P_{\mathrm{sat}}}, \tag{3}$$

where q and P_{sat} represent the modulation depth and saturation power of the SA, respectively. The OC is used to extract 20% energy of the pulse to the output. The SPS can generate an arbitrary phase distribution to fully compensate the SOD and TOD in the cavity and introduce the desired FOD. The applied phase function is[20]

$$\phi(\omega) = \sum_{n=2}^{4} \beta_n \frac{(\omega - \omega_0)^n}{n!}. \tag{4}$$

The initial parameters used for the simulation are shown in Table 1. The total SOD, TOD, and FOD of the fiber are 0.032 ps^2, 0 ps^3, and -0.0000044 ps^4, respectively. By compensating for the corresponding dispersion and introducing 0.15 ps^4 of FOD through the SPS, the PMFL can operate in the normal FOD regime. In addition, the initial signal is weak Gaussian white noise, beginning to circulate from the EDFs. The NLSE is solved numerically by the split-step Fourier method. The temporal and spectral information are recorded at the OC for each roundtrip (RT).

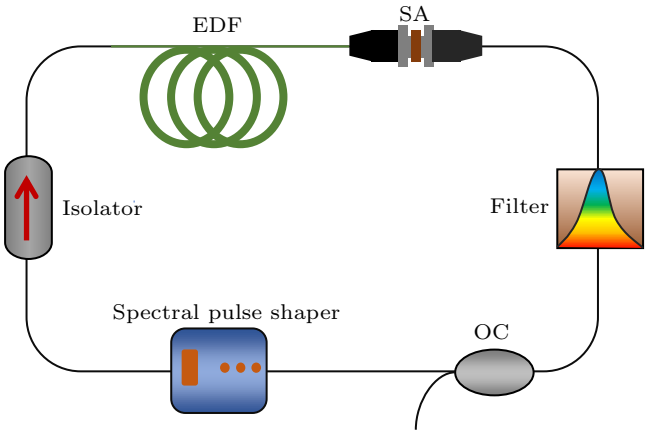


Fig. 1. PMFL model used for simulation.

Table 1. Simulation parameters.

Element	Parameter	Value
EDF	Length	2 m
	$\beta_{2-\mathrm{EDF}}$	60 ps^2/km
	$\beta_{3-\mathrm{EDF}}$	0 ps^3/km
	$\beta_{4-\mathrm{EDF}}$	0.0022 ps^4/km
	$\gamma_{-\mathrm{EDF}}$	0.006 $\mathrm{W}^{-1}\cdot\mathrm{m}^{-1}$
	g	1.5 m^{-1}
	E_{sat}	10 pJ
	Ω_{g}	30 nm
SMF	Length	4 m
	$\beta_{2-\mathrm{SMF}}$	-22 ps^2/km
	$\beta_{3-\mathrm{SMF}}$	0 ps^3/km
	$\beta_{4-\mathrm{SMF}}$	-0.0022 ps^4/km
	$\gamma_{-\mathrm{SMF}}$	0.0015 $\mathrm{W}^{-1}\cdot\mathrm{m}^{-1}$
SA	q	0.4
	P_{sat}	50 W
SPS	β_2	-0.032 ps^2
	β_3	0 ps^3
	β_4	0.1500044 ps^4

3. Result and discussion

3.1. Laser output without the filter

In our simulation, the pump power is closely linked to E_{sat}. When E_{sat} is set to 10 pJ and no spectral filter is employed, the laser outputs dissipative PQSs, as shown in Fig. 2. Figures 2(a) and 2(b) show the temporal and spectral evolutions over 1000 RTs, respectively, where stable dissipative PQSs form from weak noise after short RTs. To further characterize dissipative PQSs, the single-shot temporal and spectral distributions at the 1000th RT are extracted. In Fig. 2(c), the pulse exhibits a symmetric, broadening pedestal, and the chirp increases linearly in the central portion, while it becomes almost constant near the pedestals on both sides. The corresponding spectra show similar features under the linear and logarithmic coordinates, i.e., rectangularly distributed at the edges and significantly dropped in intensity at the center, as shown in Fig. 2(d). These unique features stem from the discrepancy of the phase shift caused by FOD and self-phase modulation (SPM) at the tails,[15] which endow dissipative PQSs with a higher capacity for nonlinear phase shift.

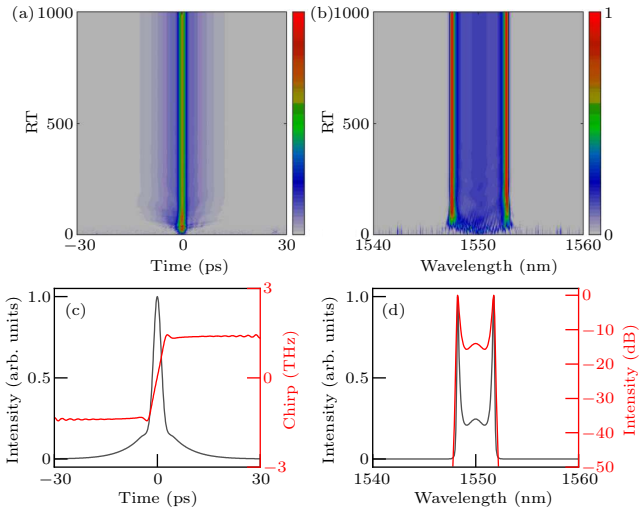


Fig. 2. Dissipative PQS output without the filter. Temporal (a) and spectral (b) evolution over 1000 RTs; single-shot time profile (c) and spectra (d) at the 1000th RT.

3.2. Laser output with the filter

In dissipative systems, multiple pulses and wave breaking are common phenomena. However, for dissipative PQSs, current studies only found wave breaking under the over-driven nonlinear effect, similar to the collapse of conventional PQSs.[26] Due to the incomplete matching of the phase shift between FOD and SPM, the formation of the pedestal broadens the pulse and creates a potential barrier at the tails. Qian *et al.* proved that when increasing the pump power, the disequilibrium of the phase shift exacerbates the energy transfer to one side of the pedestal, thus making the dissipative PQS exhibit asymmetric evolution.[15] Zhang *et al.* indicated that dissipative PQS resonance will occur if the reverse saturable absorption of the SA is considered.[23] These two phenomena suggest that the temporal pedestal hinders the formation of multi-solitons.

To eliminate time barriers, suitable shaping techniques are necessary. The spectral filtering effect is an important mechanism for soliton stability, soliton-type transition, and multi-pulsing formation in normal dispersion regimes. For solitons with large chirp, the spectral filter will also affect the time domain,[27] thus narrowing the pulse in both the time and frequency domains. For this purpose, a Lorentzian filter has been added to the cavity, whose transfer function is $F(\omega) = 1/\{1 + [(\omega - \omega_0)/\Delta\omega]^2\}$. ω_0 is the center angular frequency and $\Delta\omega$ is the filter bandwidth expressed in angular frequency. $\Delta\omega$ is set to 5 ps^{-1}, and the center wavelength at which the filter operates is 1550 nm. As shown in Figs. 3(a) and 3(b), the spectral and temporal evolution over 100 RTs describes the transition process from dissipative PQSs to new shaping solitons, where the filter was added at the 50th RT. The whole shaping process lasts for about 10 RTs. During this process, the spectral peaks on both sides are diminished, and the spectrum is contracted into a shape with a strong center and weak sides. The pulse is also compressed, and energy transfers from the low-intensity pedestal to the central portion, forming a pulse with a narrower width and higher intensity. Figures 3(c) and 3(d) exhibit the single-shot spectra and time profiles before and after adding the filter, where the purple dotted line represents the filter transmission curve. It is observable that the filter has higher transmittance near the center wavelength, guiding the spectral evolution in the cavity toward a Gaussian-like profile. The intensity of the pedestal is progressively attenuated and ultimately eliminated, which culminates in the formation of a novel pulse.

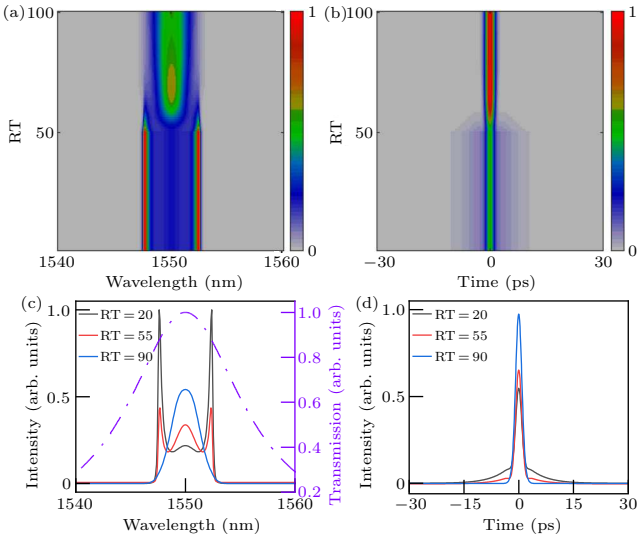


Fig. 3. Soliton transition with the filter. Spectral (a) and temporal (b) evolution, the filter was added to the cavity at the 50th RT; single-shot spectra (c) and time profile (d) at the specific RTs, the purple dotted line represents the filter transmission curve.

Increasing E_{sat} gradually enables the solitons after shap-

ing to split and tightly bind to form PQS molecules, as shown in Fig. 4. Figures 4(a) and 4(b) show the temporal and spectral evolution of bound-state two-PQSs over 1000 RTs, with $E_{\text{sat}} = 55$ pJ. The laser parameters constitute a fixed soliton attractor, i.e., it evolves toward the same steady state regardless of random noise or initial state.[28] In the initial stage, there are multiple weak noise evolutions, and the left soliton is accompanied by dispersive wave emission. Driven by the saturation absorption as well as the gain recovery effect, the noise eventually evolves into two identical PQSs. By further increasing E_{sat}, the number of solitons becomes 3, 4, and 5 sequentially, and the corresponding evolutions are shown in Figs. 4(c)–4(h). The intracavity energy determines the soliton numbers that evolve from the background weak noise to stable states, which is a result of the soliton energy quantization and gain transfer.[29] Figures 4(i) and 4(j) present the temporal and spectral distributions at the 1000th RT. As the number of pulses increases, the separation between them is not strictly equal, and the spectrum manifests asymmetric distributions, depending on the inter-pulse interaction forces. Figure 4(k) illustrates the relationship between E_{sat} and soliton number, showing a stepwise increase in the number of pulses. However, if E_{sat} is increased above 220 pJ, the intensified soliton interactions and the accumulation of nonlinear phase shifts will cause the collapse of PQS molecules.

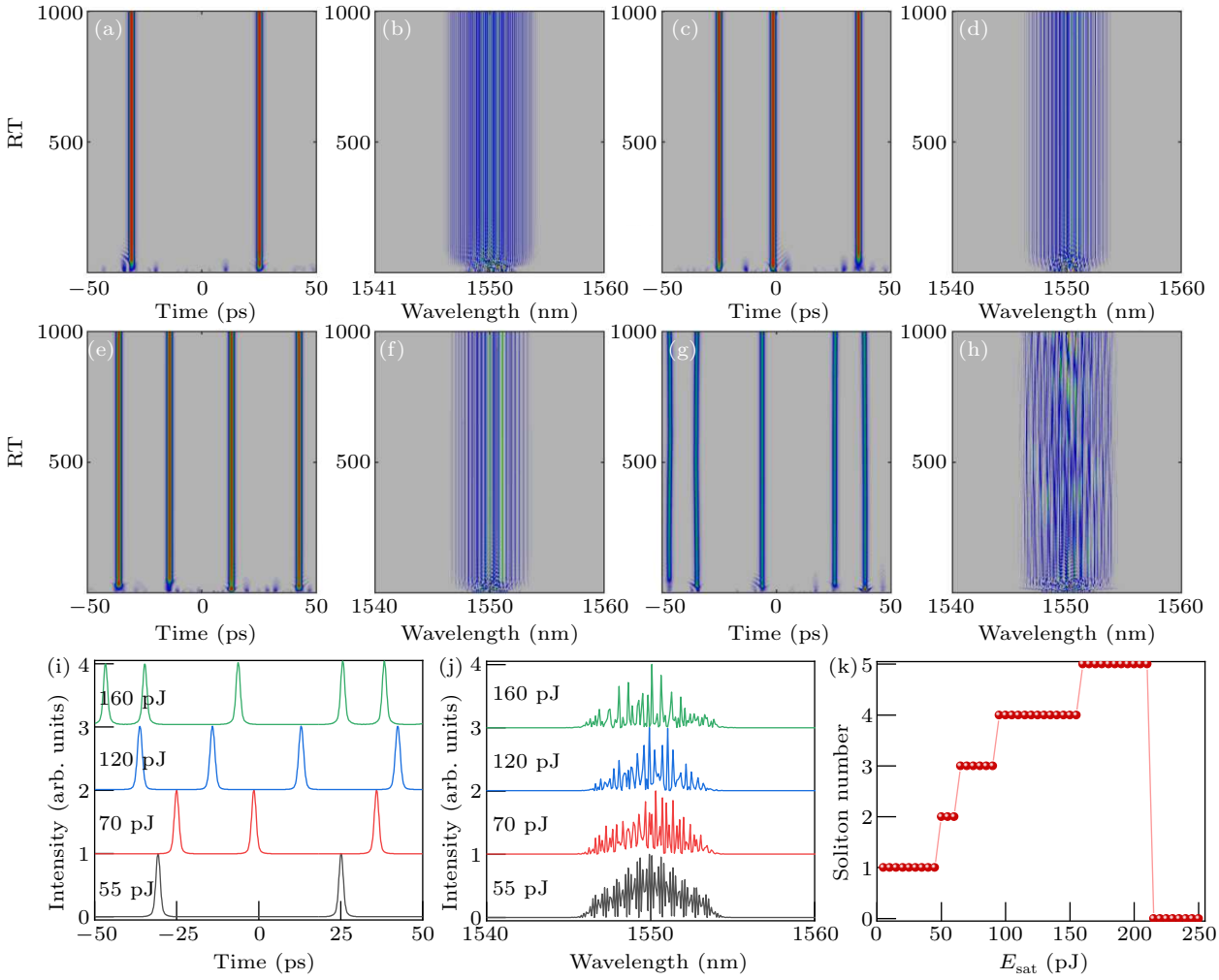


Fig. 4. Characterization of PQS molecules with different E_{sat}. (a) $E_{\text{sat}} = 55$ pJ, two pulses; (c) $E_{\text{sat}} = 70$ pJ, three pulses; (e) $E_{\text{sat}} = 120$ pJ, four pulses; (g) $E_{\text{sat}} = 160$ pJ, five pulses; the corresponding spectral evolutions (b), (d), (f), and (h); time profiles (i) and spectra (j) of the 2–5 solitons at the 1000th RT; (k) soliton number versus E_{sat}.

3.3. Influence of the effective spectral filtering effect on chaotic PQSs

The growth of the soliton number is the consequence of energy quantization that exceeds the splitting threshold, and the critical threshold is clearly defined in a fixed laser system. When the inherent gain bandwidth of the EDF is sufficiently large, it fails to impose adequate constraints on the spectral broadening caused by SPM, so that solitons like self-similarity can broaden exponentially in gain medium without splitting.[30] Therefore, adding a bandwidth-limited filter to provide spectral loss is necessary for both the generation of multiple solitons[31,32] and the management of pulse states.[27,33] When the saturation gain is large enough, the filtering supplies extra loss for spectral bandwidth, which lowers

the splitting threshold and has direct influence on the coherent recovery of unstable states.[34] For example, PQSs will collapse into a chaotic state under high pump power and large FOD conditions. By reducing the filter bandwidth to enhance the effective spectral filtering effect, it can transition to multi-pulsing states, as shown in Fig. 5.

Stable PQS molecules cannot be generated when the intracavity pump power is high enough to accumulate a large amount of nonlinearity, as shown in Fig. 4(k). While taking $E_{\rm sat} = 250$ pJ, the temporal and spectral evolutions are depicted in Figs. 5(a) and 5(b), where a pulse collides after being attracted to an adjacent pulse or a pulse recovered from noise. This dynamic process continues incessantly, leading to a chaotic evolution of multiple solitons. For large FOD, the chaos stems from the inability of the filter to supply sufficient shaping effect to compensate for the imbalance between FOD and nonlinearity. Figures 5(c) and 5(d) display the temporal and spectral evolution, respectively, by reducing $E_{\rm sat}$ to 120 pJ and increasing the intracavity β_4 to 0.5 ps^4. The temporal oscillating tail becomes longer, accompanied by non-periodic pulsating. To further investigate the impact of FOD on PQS molecules, the variation of soliton number with β_4 is shown in Fig. 5(e). Contrary to the effect of $E_{\rm sat}$, continuously increasing β_4 leads to a stepwise decrease in soliton number and eventual entry into the chaotic state. The spectra with $\beta_4 = 0.1$ ps^4, 0.3 ps^4, 0.5 ps^4 are extracted sequentially, as shown in Fig. 5(f). It can be observed that the spectrum of PQS narrows in the presence of large FOD, thus weakening the filtering effect and causing chaos when the filter bandwidth is fixed.

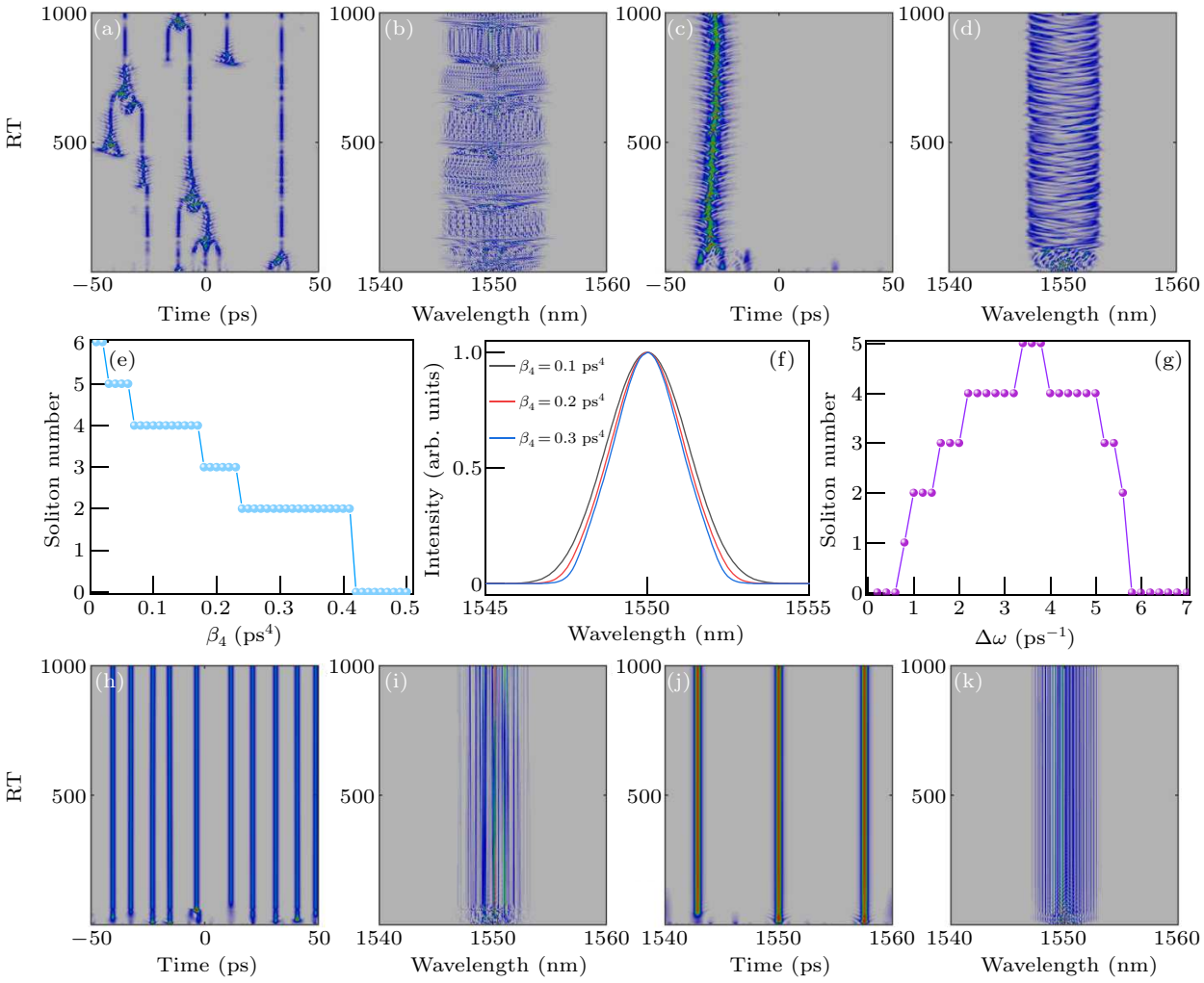


Fig. 5. Coherent recovery from chaotic PQSs to PQS molecules. Temporal [(a), (c)] and spectral [(b), (d)] evolution of chaotic PQS with high pump power $E_{\rm sat} = 250$ pJ and with large FOD $\beta_4 = 0.5$ ps^4, respectively; (e) soliton number versus intracavity FOD β_4; (f) spectral distributions with different FOD; (g) soliton number versus $\Delta\omega$; temporal [(h), (j)] and spectral [(i), (k)] evolution of coherent PQS molecules with high pump power and with large FOD, respectively, after adjusting $\Delta\omega$ from 5 ps^{-1} to 3.5 ps^{-1}.

The narrow filtering bandwidth is favorable for generating multiple solitons, provided that the filtering loss can be balanced by gain recovery. Figure 5(g) displays the soliton number versus the filter bandwidth $\Delta\omega$, and soliton molecules and stabilizing solitons cannot be obtained when $\Delta\omega$ is either too small or too large. The former results from excessive filtering loss, while the latter fails to create effective spectral filtering due to the wide filtering bandwidth. By reducing $\Delta\omega$ from

5 ps^{-1} to 3.5 ps^{-1}, the enhanced effective spectral filtering effect favors the recovery of PQS molecules, i.e., the chaotic PQS induced by high pump power can transform into coherent 10 pulses, as shown in Figs. 5(h) and 5(i). Furthermore, the chaotic PQS with large FOD can also be restored to the PQS molecule consisting of three pulses, as shown in Figs. 5(j) and 5(k). This operation for the filter not only facilitates the coherent restoration of chaotic PQSs but also markedly augments the number of PQSs that the PMFL can support.

3.4. Influence of the filter characteristic on output

The transmission curve of the filter is pivotal for wavelength selection and soliton shaping. In the case of dissipative PQSs, the spectra are symmetrically distributed around the central wavelength. The applied bandpass filter can exert equivalent loss on both sides of the spectral peaks and pulses. One operation to investigate the impact of applying asymmetric loss is to misalign the central wavelength of the filter from that of spectra, as shown in Fig. 6(a). The central wavelength ω of the filter is 1548.9 nm, with the high-transmission region shifted towards shorter wavelengths. Under the initial parameter conditions, the laser emits PQSs with an asymmetric distribution in both the time and spectral domains with $E_{\mathrm{sat}} = 20$ pJ. While E_{sat} is increased to 60 pJ, asymmetric PQS molecules consisting of two pulses can be generated. The pedestal exists on one pulse side as the filter selectively removes the spectral peaks on the right side of dissipating PQSs. This distribution feature resembles that of the dissipative PQSs in Ref. [14], with the difference that PQS molecules with shifted evolution can be generated when we further increase the pump power. Figures 6(d) and 6(f) capture the temporal evolution of shifted PQSs and PQS molecules over 1000 RTs, and the corresponding spectral evolution is displayed in Figs. 6(e) and 6(g). The pulses exhibit a certain degree of displacement during the evolution, while the spectral stability illustrates the consistency of the pulse structure. If ω_0 is adjusted to a longer wavelength over 1550 nm, the shifted direction is opposite to this result. The splitting of PQSs conveys a crucial message that the asymmetric characteristics are caused by the filter together with the imbalance between FOD and nonlinearity, which emphasizes the shaping effect of effective spectral filtering on dissipative PQSs.

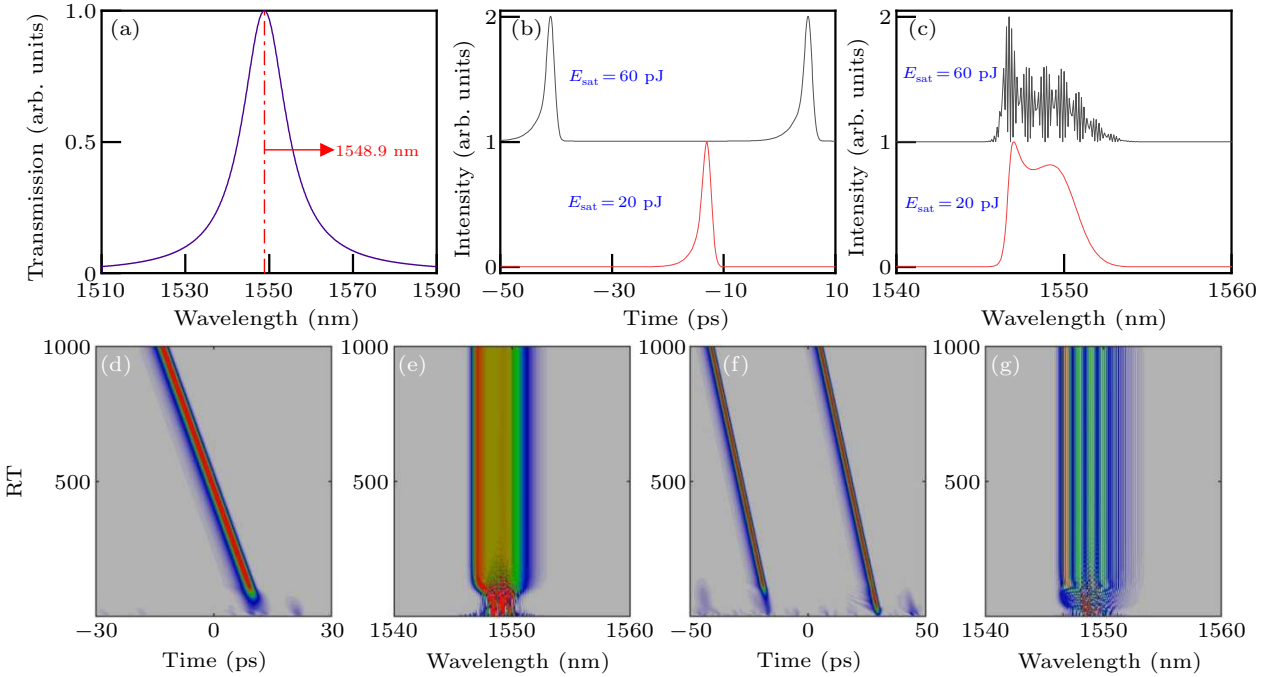


Fig. 6. Output characteristics of changing ω: (a) filter transmission curve; temporal (b) and spectral (c) distribution of asymmetric PQSs and PQS molecules; temporal evolution of asymmetric PQS (d) and PQS molecules (f) over 1000 RTs; (e) and (g), the corresponding spectral evolution, respectively.

4. Conclusion

In conclusion, we numerically investigated the role of filters in shaping the PQS at normal FOD regimes. The spectral loss filtering simultaneously acts on the time and frequency domains, thereby eliminating the original temporal pedestal that impeded dissipative PQSs from splitting. By increasing the pump power, bound-state PQS molecules comprising 2 to 5 pulses can be sequentially obtained. In addition, under conditions of large FOD and high power, the coherent restoration of chaotic PQSs to multi-pulsing states can be facilitated by reducing the filter bandwidth to enhance effective spectral filtering. Finally, altering the central wavelength of the filter to impose different transmission losses on shorter and longer wavelengths enables the formation of shifted-evolving PQSs

and PQS molecules. These results highlight the pivotal impact of spectral filtering in manipulating PQSs in normal FOD, which offers valuable insights into the flexible control of PQSs and the construction of harmonic PQS lasers.

Acknowledgment

Project supported by the National Natural Science Foundation of China (Grant No. 62175116).

References

[1] Choudhury D, Macdonald J R and Kar A K 2014 *Laser Photonics Rev.* **8** 827
[2] Sugioka K and Cheng Y 2014 *Light Sci. Appl.* **3** e149
[3] Keller U 2003 *Nature* **424** 831
[4] Fortier T and Baumann E 2019 *Commun. Phys.* **2** 153
[5] Newbury N R and Swann W C 2007 *J. Opt. Soc. Am. B* **24** 1756
[6] Udem T, Holzwarth R and Hänsch T W 2002 *Nature* **416** 233
[7] Pang M, He W, Jiang X and Russell P S J 2016 *Nat. Photonics* **10** 454
[8] Marcucci G, Pierangeli D and Conti C 2020 *Phys. Rev. Lett.* **125** 093901
[9] Rohrmann P, Hause A and Mitschke F 2012 *Sci. Rep.* **2** 866
[10] Yu T, Golovchenko E, Pilipetskii A and Menyuk C 1997 *Opt. Lett.* **22** 793
[11] Zhang Y H and Liu C 2024 *Chin. Phys. B* **33** 030506
[12] Blanco-Redondo A, De Sterke C M, Sipe J E, Krauss T F, Eggleton B J and Husko C 2016 *Nat. Commun.* **7** 10427
[13] Runge A F, Hudson D D, Tam K K, de Sterke C M and Blanco-Redondo A 2020 *Nat. Photonics* **14** 492
[14] Wang Z, Mao Y, Ling X and Zhang L 2024 *Opt. Laser Technol.* **171** 110353
[15] Qian Z C, Liu M, Luo A P, Luo Z C and Xu W C 2022 *Opt. Express* **30** 22066
[16] Runge A F, Alexander T J, Newton J, Alavandi P A, Hudson D D, Blanco-Redondo A and de Sterke C M 2020 *Opt. Lett.* **45** 3365
[17] Liu X and Pang M 2019 *Laser Photonics Rev.* **13** 1800333
[18] Wang Z, Nithyanandan K, Coillet A, Tchofo-Dinda P and Grelu P 2019 *Nat. Commun.* **10** 830
[19] Zhang Z X, Luo M, Liu J H, Yang Y T, Li T J, Liu M, Luo A P, Xu W C and Luo Z C 2024 *Nat. Commun.* **15** 6148
[20] Han Y, Gao B, Wen H, Ma C, Huo J, Li Y, Zhou L, Li Q, Wu G and Liu L 2024 *Light Sci. Appl.* **13** 101
[21] He C, Zhu Z, Yang S, Wang N, Yang Y and Lin X 2024 *Opt. Express* **32** 11895
[22] Yang S, Zhu Z, Qi Y, Jin L, Li L and Lin X 2023 *Chaos Soliton. Fract.* **172** 113544
[23] Zhang Y, Jin C, Tao C, Luo S, Ling Q, Guan Z, Chen D and Cui Y 2023 *Opt. Commun.* **538** 129479
[24] Han Y, Gao B, Wu G, Huo J Y, Wen H L, Li Y Y, Liu L and Ma C Y 2023 *Opt. Express* **31** 1787
[25] Liu L, Han Y, Huo J, Wen H, Wu G and Gao B 2023 *Chin. Phys. B* **32** 114209
[26] Yang S, Zhu Z, He C, Shi Y, Yang Y and Lin X 2024 *Chaos Soliton. Fract.* **180** 114538
[27] Wang Z, Zhan L, Fang X and Luo H 2017 *J. Opt. Soc. Am. B* **34** 2325
[28] Zhang J H, Qin H Q, Si Z Z, Jia Y H, Kudryashov N A, Wang Y Y and Dai C Q 2024 *Chaos Soliton. Fract.* **187** 115380
[29] Tang D, Zhao L M, Zhao B and Liu A 2005 *Phys. Rev. A* **72** 043816
[30] Chong A, Wright L G and Wise F W 2015 *Rep. Prog. Phys.* **78** 113901
[31] Haboucha A, Komarov A, Leblond H, Sanchez F and Martel G 2008 *Opt. Fiber Technol.* **14** 262
[32] Yang S, Zheng J, Qi Y, Shi Y, Li D, Nie X and Sun Z 2023 *Opt. Laser Technol.* **157** 108726
[33] Khanolkar A and Chong A 2020 *Opt. Lett.* **45** 6374
[34] Wen Z, Lu B, Qi X, Zhang C, Wang K, Chen H and Bai J 2019 *J. Opt. Soc. Am. B* **36** 952